Sensors and Actuators A 163 (2010) 383–387

Contents lists available at ScienceDirect

Sensors and Actuators A: Physical

journal homepage: www.elsevier.com/locate/sna

# AFM characterization of nanopositioner in-plane stiffnesses

Seung Ho Yang[a,*], Yongsik Kim[a], Kavuri Premsagar Purushotham[b], Jae-Myung Yoo[a], Young-Man Choi[a], Nicholas Dagalakis[a]

[a] Intelligent Systems Division, National Institute of Standards and Technology, 100 Bureau Drive, Gaithersburg, MD 20899-8230, United States
[b] Precision Engineering Division, National Institute of Standards and Technology, 100 Bureau Drive, Gaithersburg, MD 20899-8212, United States

ARTICLE INFO

*Article history:*
Received 1 February 2010
Received in revised form 29 June 2010
Accepted 9 July 2010
Available online 16 July 2010

*Keywords:*
AFM
Colloidal probe
In-plane stiffness
MEMS
Nanopositioner

ABSTRACT

A versatile method for measurement of in-plane stiffness of micro-elements was developed and its usefulness has been demonstrated. The in-plane stiffness of a NIST nanopositioner has been measured directly using a colloidal probe in an AFM without any fixture. Using this method it was possible to measure the in-plane stiffness at different locations of the same micro-element. The in-plane stiffness ratio of a microlever system was also measured and a good agreement was found between the calculated and measured values. Further, when the minimum width of flexures is 4 μm, the measured in-plane stiffnesses showed a close agreement with the calculated value.

Published by Elsevier B.V.

## 1. Introduction

Direct measurement of the mechanical responses of micro- and nanoscale elements has been a challenge in microelectro-mechanical systems (MEMS) and nanoelectro-mechanical systems (NEMS) [1]. Although one may possibly predict those mechanical responses with finite element methods [2] it is not practically possible to utilize them for designing the small scale elements directly. This is because of the wide variation in the mechanical properties across the crystallographic directions, variation in density, fabrication methods and lack of cross wafer uniformity.

Webber et al. [3] selected 101 microscale samples from the same wafer and measured out-of-plane stiffnesses. For the same sample dimensions they found that the stiffness varied widely over a factor of two. Further, they observed that there was no systematic correlation between the measured stiffness and the resonance frequency. They attributed this behavior to the non-uniformity of composition and material properties in the thinnest elements. Thus the stiffness estimation method based on the assumption of uniformity of material properties would lead to errors. Drummond and Senden [4] also found that Young's modulus of silicon nitride films varied by a factor of two between wafers.

When multiple MEMS elements are fabricated on a wafer, the accuracy of the critical dimensions across various elements in the wafer, is essential. But it is very common for a processed wafer to exhibit non-negotiable cross wafer variations. It is reported [5] that variations of as much as 10% from one side of the wafer to the other are common. Deep reactive ion etching (DRIE) exhibits significant variations in etch rates between the center and edge of a wafer. The variation results in a gradient in etch depth [5]. Yeo et al. [6] observed cross wafer variation in their investigation. Li et al. [7] also observed that imperfections in etched vertical shapes cannot be avoided during the fabrication processes that use DRIE.

In order to measure the stiffness of the MEMS elements, researchers have used custom-made fixtures and apparatus. Miyamoto et al. [8] used a servo-controlled balance. They attached the MEMS spring vertically to the balance apparatus and measured stiffness. Chasiotis and Knauss [9] measured out-of-plane stiffness using a load cell and a calibrated inchworm. Chu and Zhang [10] measured in-plane stiffness of a micro- element using a micro-tensile tester. The micro-tensile tester consisted of a piezoelectric actuator, a load cell, an inductance displacement sensor, a 5-axis translation stage and a microscopic imaging system. These custom-built apparatuses are usually large in size and are not versatile so that one has to manufacture another apparatus when properties of different shapes and sizes must be measured.

A more versatile approach to measure stiffness of micro-elements could be the use of nanoindentors. McFarland and Colton [11] and Tay et al. [12] measured the out-of-plane stiffness of a micro-element using a nanoindentor. The nanoindentor allows one to measure force and displacements of micro-elements without any special fixtures. However, only the out-of-plane stiffnesses

* Corresponding author.
*E-mail address:* seungho@cme.nist.gov (S.H. Yang).

0924-4247/$ – see front matter. Published by Elsevier B.V.
doi:10.1016/j.sna.2010.07.006

are reported to be measured successfully with the nanoindentors.

Recently the atomic force microscope (AFM) was used to measure directly small scale mechanical responses. In the MEMS and NEMS, the AFM was used for measuring force and displacement. AFM was successfully used to measure out-of-plane stiffness of MEMS elements [13], of out-of-plane stiffness of micro-beams [14], and out-of-plane resonance frequency of a microresonator [15]. Gates and Reitsma [16] conversely measured the AFM cantilever out-of-plane stiffness using a MEMS cantilever array. However, the in-plane stiffness measurement on MEMS elements with AFM has not been reported.

Mueller-Falcke et al. [17] measured force and displacement on a vertically positioned MEMS element using a fixture in which the MEMS element was mounted vertically in a nanoindentor. This is not generally possible because not all MEMS elements have an open ended structure.

In this work we report the direct measurement of the in-plane stiffness of NIST's nanopositioner [18] using a colloidal probe in an AFM without any fixture. This method is so versatile that it enables one to measure the in-plane stiffness at different locations of the same sample. Using this method the in-plane stiffness ratio of the microlever system is also measured and analyzed.

## 2. Experimental details

### 2.1. Colloidal probe fabrication and lateral stiffness calibration

A colloidal probe was utilized because the spherical particle automatically defines the contact direction and does not generate a force component in the out-of-plane direction.

A colloidal probe was prepared by gluing (Loctite, QuickSetth Epoxy25)[1] a glass sphere (NIST, SRM 1003C25) onto a silicon cantilever (Veeco, TESP) as shown in the scanning electron micrograph in Fig. 1. A silicon grating sample (TGT 01, NT-MDT25) was scanned with the colloidal probe in order to determine its radius, and the radius was found to be 20 μm.

Since the surface contamination and adhesion may play a role during the tilt of the colloidal probe [19], the colloidal probe was plasma cleaned (Harrick Plasma Cleaner, PDC-00125) for 30 s to eliminate possible contamination from the grating sample. After plasma cleaning, the torsional stiffness of the colloidal probe was calibrated and the probe was used for direct measurement of in-plane stiffness.

The torsional stiffness of the colloidal probe was calibrated by laterally pushing a reference cantilever of known bending stiffness ($k$). The detailed calibration method is reported elsewhere [20]. For the probe cantilever used in this work, calibration with a reference cantilever (silicon, $k = 67 \pm 1.0$ nN/nm) showed that it had a torsional stiffness of $10.8 \pm 0.17$ mN/rad.

### 2.2. NIST's nanopositioner and the fabrication procedure

The NIST nanopositioners are developed to control the optical path with the nanometer accuracy. A scanning electron microscope (SEM) image of the NIST MEMS Nanopositioner [18] is presented in Fig. 2(a). The stage was suspended with micro-flexures and one such flexure is shown in Fig. 2(b). One side of the stage plate was connected to a pair of microlevers which were connected to the rigid Si body by two flexure mechanisms. The other side of the plate was connected to the micro-thermal actuator with a pair of microlevers mechanism. The calculated actuation ratio was 10.86 resulting in a magnification of the stroke of the micro-thermal actuator by the same factor. With this arrangement it was possible to move the stage plate with an accuracy of ±7 nm [21].

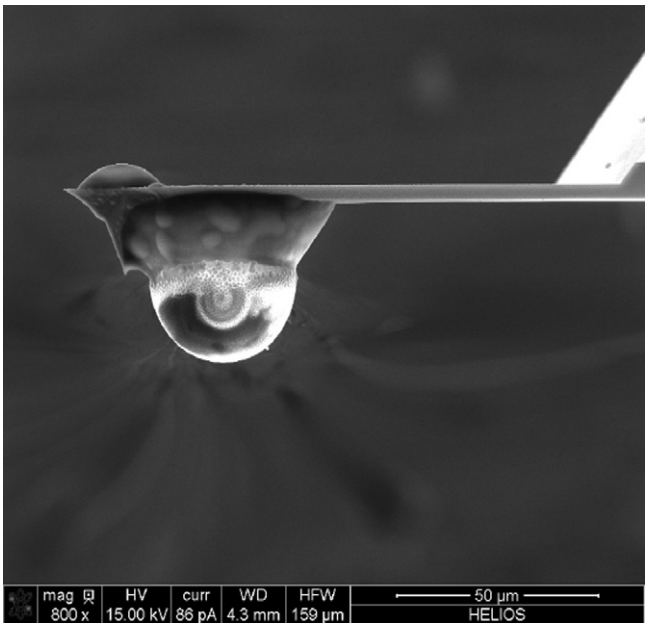


**Fig. 1.** Scanning electron micrograph of the colloidal probe. Horizontal field width 159 μm.

The various steps in the fabrication process of the nanopositioner are presented in Fig. 3. A silicon-on-insulator (SOI, Ultrasil Co.) with device layer thickness of 25 μm, buried oxide thickness of 1 μm and the handle layer thickness of 400 μm was used. The wafer was cleaned in a cleaning bath (Reynoldstech Co.) followed by spin rinse drying (Semitool PSC-101) and is depicted in Fig. 3(a). The cleaned wafer was spin coated with photoresists (LOR-5A; MicroChem and SPR 200-3; MicroChem) and exposed using broad band optical lithography (MA6, Suss Microtech). Then the exposed wafer was developed using MF-26A (Microdeposit Co.). Using an E-Beam Evaporator (Infinity 22, Denton) Cr (50 nm in thickness) and Au (500 nm in thickness) were deposited on the wafer to make metal pads. Then the residual Cr/Au and photoresist layers were removed using the lift-off technique. Fig. 3(b) shows the deposited metal pad (Cr/Au) on the wafer. The wafer was then spin coated with photoresists (HMDS (hexamethyldisilazane); MicroChem Co. and SPR 220-3; MicroChem Co.) and exposed using a broad band optical lithography (MA6, Suss Microtech). The exposed wafer was developed using MF-26A (Microdeposit Co.). Then deep reactive ion etching (DRIE; Shuttleline DSE II, Unaxis Co.) was used for the front side to get the shape of the nanopositioner. This is depicted in Fig. 3(c). The backside of the wafer was worked on. The back of the wafer was spin coated with photoresists (HMDS; MicroChem and SPR 220-7; MicroChem), exposed with the broadband lithography (MA6, Suss Microtech) and developed with MF-CD-26A (MicroChem). Then the wafer was subjected to DRIE (Shuttleline DSE II, Unaxis Co.). This is depicted in Fig. 3(d). Then the buried oxide was removed using buffered-oxide etch (BOE) solution (1178, J.T. Baker). This is shown in Fig. 3(e).

### 2.3. Removing micro-thermal actuator

In order to modify the actuation distance and accuracy of the nanopositioner, it is essential to know the stiffness of the nanopo-

[1] Certain instruments and materials are identified to adequately specify the experimental procedure. Such identification does not imply recommendation or endorsement by the National Institute of Standards and Technology, nor does it imply that the materials or instruments identified are necessarily the best available for the purpose.

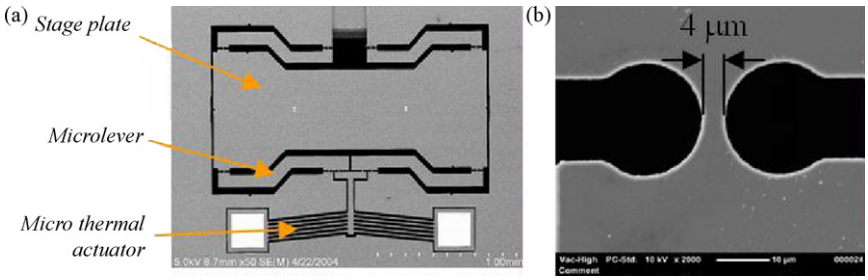


**Fig. 2.** Scanning electron microscopic images of (a) NIST's nanopositioner (horizontal field width (HFW) 2.48 mm) and (b) the flexure (horizontal field width (HFW) 57 μm).

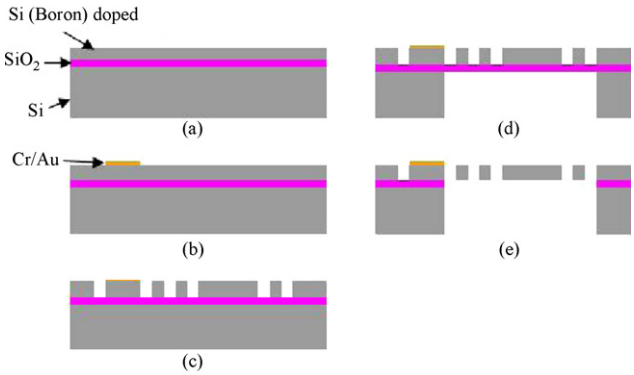


**Fig. 3.** Graphical representation on fabrication processes of NIST's nanopositioner: (a) cleaned SOI wafer, (b) metal pad (Cr/Au) deposition, (c) front side DRIE, (d) back side DRIE, (e) removing buried silicon oxide layer with BOE.

sitioner without the actuator. After the fabrication process, the micro-thermal actuator was removed from the nanopositioner so that the mechanical properties of the stage could be measured independently from the actuator. To remove the actuator, the connecting arm between the micro-actuator and the microlever was cut using focused ion beam (FIB). The cutting was performed in a Helios Dual Beam SEM (FEI Co.) using focused gallium ions. This is shown in Fig. 4(a and b). Fig. 4(c) shows the optical micrograph of the nanopositioner without the arms of the thermal actuators. After the FIB cutting of the arm, the thermal actuator part was removed by pressing it with an etched tungsten tip.

## 3. Out-of-plane stiffness measurement with AFM

The out-of-plane stiffness of NIST's nanopositioner was measured using AFM (Multimode, Nanoscope IIIa, Veeco) with a colloidal probe. Before making these measurements the vertical bending stiffness of the colloidal probe was calibrated and was found to be $42 \pm 0.5$ N/m. The details of calibration method are given in Ref. [16].

**Table 1**
Measured out-of-plane stiffnesses ($K_O$) and the uncertainties of the NIST nanopositioner.

| Location | 1 | 2 | 3 | 4 | Center |
|---|---|---|---|---|---|
| $K_O$ (nN/nm) | 25.9 | 27.8 | 26.4 | 25.0 | 64.4 |
| Uncertainty (%) | <5% | <5% | <5% | <5% | <5% |

Force–distance curves were obtained by pushing the nanopositioner stage and the rigid body with the calibrated probe. Using the known stiffness of the cantilever and sensitivities of the stage and the rigid body the out-of-plane stiffness of nanopositioner stage was calculated. Details of the measuring methods are summarized in references [13–16]. The various locations at which out-of-plane stiffness was measured are shown in Fig. 5 and the results are given in Table 1.

## 4. In-plane stiffness measurement with AFM

The various stages in the measurement of in-plane stiffness are presented graphically in Fig. 6. Keeping the cantilever stationary the nanopositioner was moved laterally. On contact the stage fixtures and the cantilever are deformed. When the stage was moved back, the cantilever and the stage flexures returned to their original position. This is illustrated in Fig. 6(a)–(c).

Before lateral contact (Fig. 6b), the location of laser spot on the laser diode is not a function of the lateral movement of the stage. But, after the stage is brought into contact (Fig. 6c), the location of the laser spot becomes a function of the lateral movement of the stage. Therefore using a colloidal probe with a calibrated torsional stiffness, it is possible to calculate the in-plane stiffness of the nanopositioner by measuring the laser spot movement.

Pushing the colloidal probe laterally with the stage results in torsion of the probe (Fig. 6c). The lateral sensitivity $C_L^{stage}$ for this experiment can be obtained from the slope of the plot of lateral cantilever deflection vs. lateral moving distance of PZT head (Fig. 6a). Repeating this sensitivity measurement using a rigid edge yields sensitivity $C_L^o$. The forces acting on the side of the colloidal probe are in equilibrium (Fig. 6c), i.e., $k_s d_s = k_p d_p$, where $k_s$ and $k_p$ are the

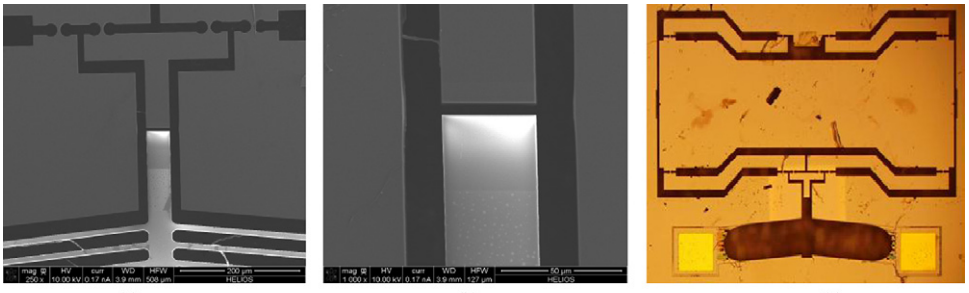


**Fig. 4.** SEM images of the NIST's nanopositioner after FIB cutting of the connecting arm between the stage and the thermal actuator (a and b) and an optical micrograph of the nanopositioner after removing the thermal actuator (c).

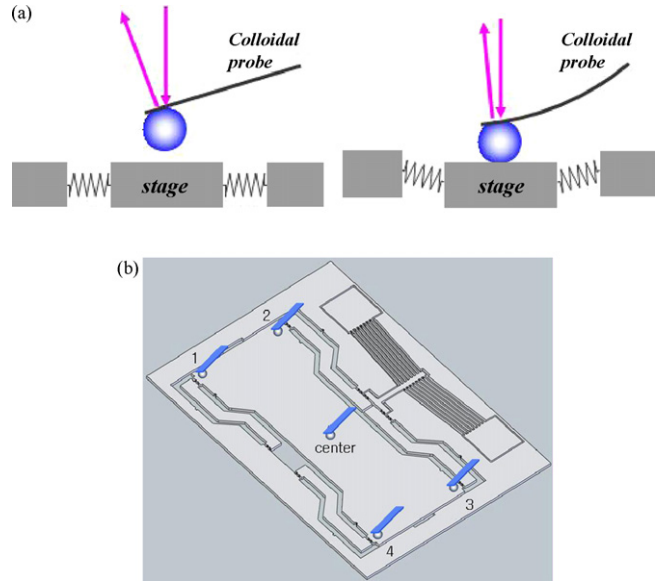


**Fig. 5.** Graphical illustration of the out-of-plane stiffness measurement: (a) the colloidal probe and the stage without loading, (b) contact between the colloidal probe and the stage with load, (c) graphical configuration of the measurement locations.

**Table 2**
Measured in-plane stiffnesses ($K_i$) and the uncertainties of NIST's nanopositioner.

| At location "A" | | At location "B" | |
|---|---|---|---|
| $K_i$ (nN/nm) | Uncertainty (%) | $K_i$ (nN/nm) | Uncertainty (%) |
| 39.5 | <±5 | 4537.4 | <±5 |

in-plane stiffnesses of the stage and the colloidal probe, $d_s$ and $d_p$ are the in-plane moving distances of the stage and the probe respectively. Furthermore, when $\Delta U_L$ is the lateral voltage from the quad-cell detector resulting from the distortion of the colloidal probe ($d_p$) and the deformation of the stage ($d_s$), the sensitivity of the stage is given by $C_L^{stage} = (d_s + d_p)/\Delta U_L = C_L^o + d_s/\Delta U_L$. Expressing $d_p$ and $d_s$ in terms of $k_p$ and $k_s$, we have

$$k_s = \left( \frac{C_L^o}{C_L^{stage} - C_L^o} \right) k_p \quad (1)$$

The measured in-plane stiffness values (at locations "A" and "B" in Fig. 6d) and the uncertainties of the measurements are summarized in Table 2. All the measurements are repeated three times.

## 5. Discussion

The measured in-plane stiffness values listed in Table 2 were compared with finite element method (FEM) calculations. For FEM, the software used was ANSYS. For modeling the in-plane deformation of the lever of the nanopositioner, the minimum width of the flexure (Fig. 2b) is the key parameter. Even though the designed minimum width was 5 μm the actual minimum width was found to be 4 μm after fabrication. Using 5 μm as minimum width and

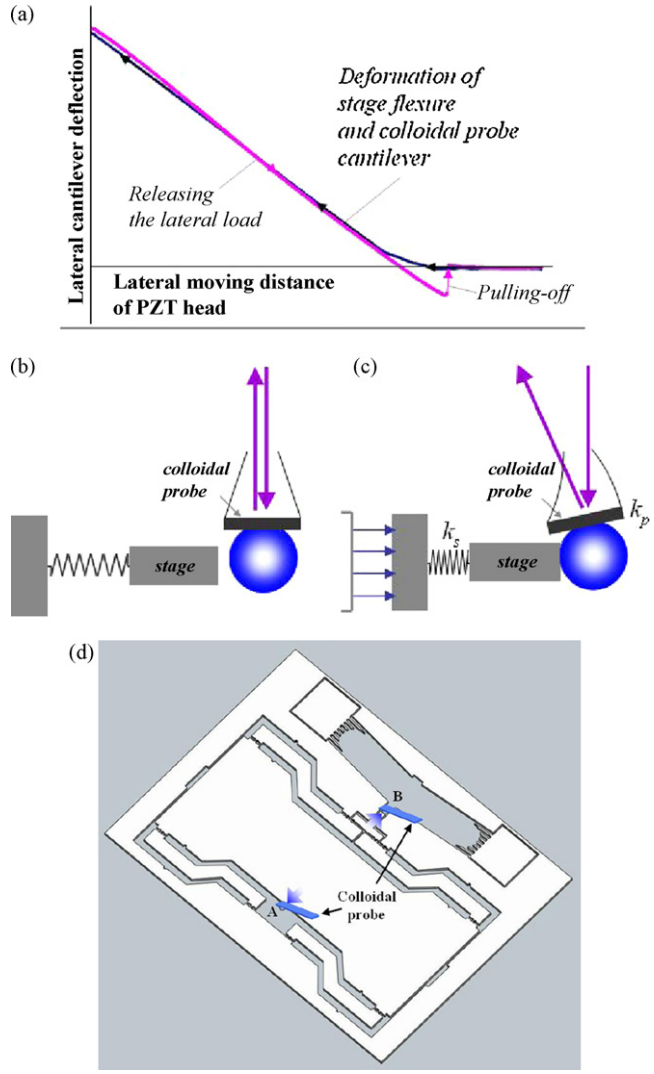


**Fig. 6.** Graphical illustration of the in-plane stiffness measurement: (a) lateral cantilever deflection signal as function of the lateral moving distance of a PZT head, (b) the colloidal probe and the stage without lateral loading, (c) contact between the colloidal probe and the stage with lateral load, (d) graphical configuration of the measurement locations (the shaded block arrows present the lateral loading direction onto the colloidal probe).

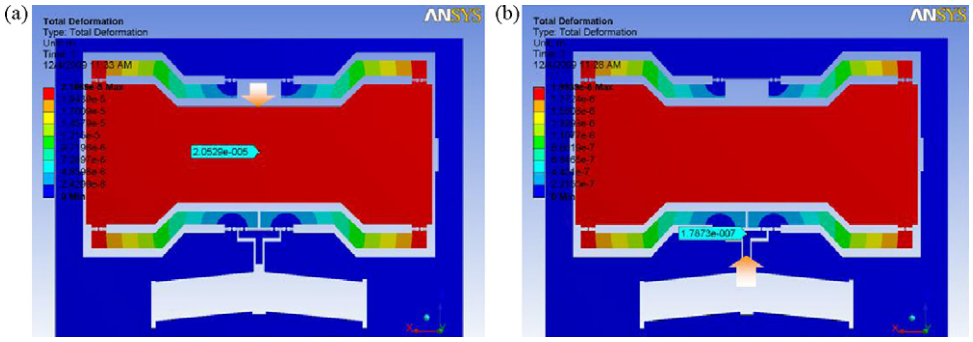


**Fig. 7.** Sample FEM results on nanopositioners which have the minimum flexure width of 4 μm (a and b) (the shaded block arrows present the lateral loading direction).

**Table 3**
In-plane stiffnesses ($K_i$) and the stiffnesss ratio of NIST's nanopositioner.

| | $K_i$ (nN/nm), at location "A" | $K_i$ (nN/nm), at location "B" | Stiffness ratio |
|---|---|---|---|
| FEM ($t^a$ = 5 μm) | 82.5 | 9225 | 111.8 |
| FEM ($t^a$ = 4 μm) | 48.7 | 5596 | 114.9 |
| Colloidal probe, AFM | 39.5[b] | 4537[b] | 114.9 |

[a] $t$ is the minimum width of the flexure.
[b] Uncertainty <±5%.

1 mN as the lateral force the FEM results showed that the moving distances at locations "A" and "B" were 12.12 μm (Fig. 7a) and 0.11 μm (Fig. 7b). And when 4 μm was used as minimum width and 1 mN as the lateral force the FEM results showed that the moving distances at locations "A" and "B" were 20.53 μm (Fig. 7c) and 0.18 μm (Fig. 7d).

The results from FEM and AFM are listed in Table 3. The "stiffness ratio" was calculated as $K_i$(at location "B")/$K_i$(at location "A").

It can be seen clearly from Table 3 that there is considerable variation in the in-plane stiffness estimated by FEM with the maximum versus minimum width of the flexure. However, if the stiffness ratio is considered, the variation is small. Further there is a good agreement between the calculated minimum flexure width (FEM) and measured (AFM) values.

Further, from Table 3 it is evident that the actual stiffness values for the same minimum flexure width (4 μm) measured (AFM) values are in close agreement with the calculated (FEM) values.

## 6. Conclusions

A versatile method for measurement of in-plane stiffness of micro-elements was developed and its usefulness has been proved. The in-plane stiffnesses of the NIST nanopositioner has been measured directly using a colloidal probe in an AFM without any fixture. Using this method it was possible to measure the in-plane stiffness at different locations of the same micro-element. The in-plane stiffness ratio of the microlever system was also measured and good agreement was found between the calculated (FEM) and measured (AFM) values. Further, for the same minimum width (4 μm), the measured (AFM) stiffness values showed a close agreement with the calculated (FEM) values.

## Acknowledgements

The authors would like to thank Dr. John Kramar and Dr. Pradeep Namboodiri from NIST for reviewing this paper and Dr. Robert Cook and Dr. Mike Shneier from NIST for their help and support.

## References

[1] T. Yi, C.-J. Kim, Measurement of mechanical properties for MEMS materials, Meas. Sci. Technol. 10 (1999) 706–716.
[2] W. Zhang, R. Baskaran, K.L. Turner, Effect of cubic nonlinearity on auto-parametrically amplified resonant MEMS mass sensor, Sens. Actuators A 102 (2002) 139–150.
[3] G.B. Webber, G.W. Stevens, F. Grieser, R.R. Dagastine, D.Y.C. Chen, Variations in properties of atomic force microscope cantilever fashioned from the same wafer, Nanotechnology 19 (2008) 105709.
[4] C.J. Drummond, T.J. Senden, Characterization of the mechanical properties of thin film cantilevers with the atomic force microscope, Mater. Sci. Forum 189–190 (1995) 107–114.
[5] M. God-el-Hak, MEMS: Introduction and Fundamentals, Taylor and Francis, 2005, pp. 11-22–11-23.
[6] J. Yeo, B. Lee, T.-Y. Lee, G. Greenburg, D. Meshulach, E. Ravid, S. Levi, K. Kan, S. Shabtay, Y. Cohen, O. Rotlevy, AWV: high throughput across array across wafer variation mapping, Proc. SPIE 6922 (2008), 69221S1–69221S9.
[7] J. Li, A.Q. Liu, Q.X. Zhang, Tolerance analysis for comb-drive actuators using DRIE fabrication, Sens. Actuators A 125 (2006) 494–503.
[8] K. Miyamoto, T. Jomori, K. Sugano, O. Tabata, T. Tsuchiya, Mechanical calibration of MEMS springs with sub-micro-Newton force resolution, Sens. Actuators A 143 (2008) 136–142.
[9] I. Chasiotis, W.G. Knauss, A new microtensile tester for the study of MEMS materials with the aid of atomic force microscopy, Exp. Mech. 42 (1) (2002) 51–57.
[10] J. Chu, D. Zhang, Mechanical characteristics of thermal $SiO_2$ micro-beams through tensile testing, J. Micromech. Microeng. 19 (2009) 095020.
[11] A.W. McFarland, J.S. Colton, Role of material microstructure in plate stiffness with relevance to microcantilever sensors, J. Micromech. Microeng. 15 (2005) 1060–1067.
[12] C.J. Tay, C. Quan, M. Gopal, L. Shen, R. Akkipeddi, Nanoindentation techniques in the measurement of mechanical properties of InP-based free-standing MEMS structures, J. Micromech. Microeng. 18 (2008) 025015.
[13] D. Bachmann, S. Kühne, C. Hierold, Determination of the adhesion energy of MEMS structures by applying Weibull-type distribution function, Sens. Actuators A 132 (2006) 407–414.
[14] B.T. Comella, M.R. Scalon, The determination of the elastic modulus of microcantilever beams using atomic force microscopy, J. Mater. Sci. 35 (2000) 567–572.
[15] S. Ryder, K.B. Lee, X. Meng, L. Lin, AFM characterization of out-of-plane high frequency microresonators, Sens. Actuators A 114 (2004) 135–140.
[16] R.S. Gates, M.G. Reitsma, Precise atomic force microscope cantilever spring constant calibration using a reference cantilever array, Rev. Sci. Instrum. 78 (2007) 086101.
[17] C. Mueller-Falcke, S.D. Gouda, S. Kim, S.-G. Kim, A nanoscanning platform for bio-engineering: and in-plane probe with switchable stiffness, Nanotechnology 17 (2006) S69–S76.
[18] J.J. Gorman, Y.-S. Kim, N.G. Dagalakis, Control of MEMS nanopositioner with nano-scale resolution, in: Proceedings of IMECE2006, Chicago, IL, November 5–10, 2006, pp. 1–9.
[19] S.H. Yang, H. Zhang, M. Nosonovsky, K.-H. Chung, Effects of contact geometry on pull-off force measurements with a colloidal probe, Langmuir 24 (2008) 743–748.
[20] S. Ecke, R. Raiteri, E. Bonaccurso, C. Reiner, H.-J. Deiseroth, H.-J. Butt, Measuring normal and friction forces acting on individual fine particles, Rev. Sci. Instrum. 72 (2001) 4164–4170.
[21] J.J. Gorman, Y.-S. Kim, A.E. Vladar, N.G. Dagalakis, Design of an on-chip micro-scale nanoassembly system, in: Proceedings of the 4th International Symposium on Nanomanufacturing (ISNM2006), 2006, pp. 160–165.